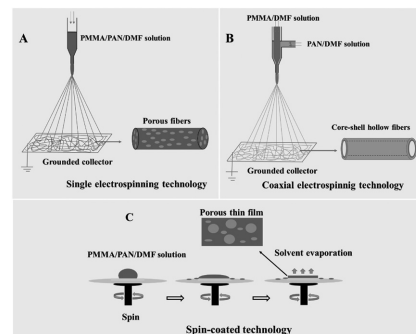


Comparatively Thermal and Crystalline Study of Poly(methyl-methacrylate)/Polyacrylonitrile Hybrids: Core–Shell Hollow Fibers, Porous Fibers, and Thin Films

Jiangnan Huang, Yonghai Cao,* Zhongyuan Huang, Samantha A. Imbraguglio, Zhe Wang, Xiangfang Peng,* Zhanhu Guo*

The polyacrylonitrile/polymethyl-methacrylate (PMMA/PAN) porous fibers, core–shell hollow fibers, and porous thin films are prepared by coaxial electrospinning, single electrospinning, and spin-coating technologies, respectively. The different morphologies arising from different processes display great influences on their thermal and crystalline properties. The adding of PMMA causes porous structure due to the microphase-separation structure of immiscible PMMA and PAN phases. The lower weight loss, higher degradation temperature, and glass-transition temperatures of porous thin films than those of porous fibers and core–shell hollow fibers are obtained, evidencing that the polymer morphologies produced from the different process can efficiently influence their physical properties. The orthorhombic structure of PAN crystals are found in the PMMA/PAN porous thin films, but the rotational disorder PAN crystals due to intermolecular packing are observed in the PMMA/PAN porous fibers and core–shell hollow fibers, indicating that different processes cause different types of PAN crystals.



J. Huang, Dr. Y. Cao, Prof. X. Peng
Laboratory of Polymer Processing Engineering
of Ministry of Education
South China University of Technology
Guangzhou, Guangdong 510640, China
E-mail: meyhcao@scut.edu.cn; pmxfpeng@scut.edu.cn

J. Huang, Dr. Y. Cao, Prof. Z. Guo
Integrated Composites Laboratory (ICL)
Department of Chemical and Biomolecular Engineering
University of Tennessee
Knoxville, TN 37996, USA
E-mail: zguo10@utk.edu

Dr. Z. Huang, S. A. Imbraguglio, Prof. Z. Wang
Department of Chemistry
Xavier University of Louisiana
New Orleans, LA 70125, USA

1. Introduction

Recently, the compound nanofibers and thin films arouse great interests in academic community.^[1–8] Nanofibers with novel secondary structures (hollow, core–shell, and porous) have extensive applications in biomedical fields, energy, and environmental engineering areas, because of their complex pore structures, high specific surface area, small diameter, and so on.^[9–13] The core–shell nanofibers have demonstrated further outstanding physicochemical properties including photocatalytic properties and flexible character.^[14–16] For example, poly(3-hydroxy butyrate) (PHB)/poly(D,L-lactic acid) (PDLA) core–shell fibers, with more sustained release of dimethylxalylglycine drug than single PDLA or PHB fibers, were used for drug delivery.^[17] And the

core-shell polymer fibers containing metal catalysts inside showed high activity in hydrogenation reductions and were easy to remove the polymer shell to recycle the expensive metal catalysts.^[18] What is more, the core-shell polysulfonamide composites nonwoven fibers, used as a lithium ion battery separator, displayed better electrolyte wettability, and superior thermal stability.^[19] The compound thin films, with 60–500 Å thickness, have been considered to be high-tech materials due to the tunable film thickness and a plenty choice of usable materials (organic and inorganic materials).^[20–23] The special micro- and nano-structure (ordered porous)^[24,25] and a wide range of available materials for coating planar and particulate substrates expanded the applications of thin films in various areas, such as optical component, energy storage, magnetic recording, and so on.^[21–23,26–28] The Cu₂O thin films showed a high performance in solar cells, with the hole density of 10¹⁷ cm⁻³.^[26] And the cellulose/poly(vinylidene fluoride-co-hexafluoropropylene) (PVDF) nonwoven thin films were proved to be an advanced separator for high-performance lithium ion battery (high ionic conductivity, electrolyte uptake, thermal resistance, and electrochemically interfacial stability).^[28]

The wide uses of polyacrylonitrile (PAN) in nanofibers and textile industry have attracted great attentions on the thermal behavior and crystallization of PAN.^[29,30] PAN, with a chain of acrylonitrile structural head-tail connecting, has high melting temperature (>300 °C), which is close to its degradation temperatures. When PAN was heated over a temperature of 180 °C in an inert atmosphere, the characteristic shrinkage (physical shrinkage and chemical shrinkage) occurred.^[31–33] The physical shrinkage leading to the relaxation of molecular orientation took place in the temperature range of 180–250 °C. The chemical shrinkage including three major exothermic reactions (cyclization of nitrile groups, dehydrogenation, and oxidation) occurred at the temperatures of 200–300 °C, which was close to its melting temperature 137 °C.^[34,35] PAN was also considered as a kind of hemicrystalline polymer, and the mechanical properties were greatly improved by its crystals.^[36]

Generally speaking, the core-shell nanofibers could be prepared by coelectrospinning of incompatible solutions (poly(ε-caprolactone)/gelatin, polymethyl-methacrylate (PMMA)/PAN).^[5,37,38] In order to produce core-shell hollow fibers by coaxial electrospinning, PMMA, which is spinnable material and incompatible with PAN, was used for core materials in electrospun fibers.^[4,5,37] What is more, PMMA/PAN homogenous composites and core-shell fibers showed high thermal stability, ionic conductivity, and electrolyte uptake in the applications of battery-separator applications.^[39,40] Usually, the hollow nanofibers were prepared by selective removal of core materials of the core-shell fibers,^[41] and the porous nanofibers were produced by immersing in a cryogenic liquid

to remove solvent in the fibers,^[42] or by removing other components in the polymer.^[43–45] The preparation of the reported core-shell hollow or porous samples included two procedures, i.e., processing and pore forming procedure.^[46] Although so many works have focused on morphologies and the application of core-shell hollow fibers, porous fibers, and thin films, there has been very little research reported on the influence of processing technologies on their thermal and crystalline properties.

In this paper, the PMMA/PAN porous fibers, core-shell hollow fibers, and porous thin films were prepared by single electrospinning, coaxial electrospinning, and spin-coating technologies, respectively. And the thermal properties and crystallization among the core-shell hollow fibers, porous fibers, and porous thin films were investigated and compared in details.

2. Experimental Section

2.1. Materials

Raw PAN powder (molecular weight ≈50 000) was purchased from Scientific Polymer Products, Inc. N,N-Dimethylformamide (DMF, anhydrous, 99.8%, 0.944 g mL⁻¹) was purchased from Sigma-Aldrich Company. Raw PMMA powder (average molecular weight ≈94600) was purchased from Acros Organics. All the chemicals were used without any treatments.

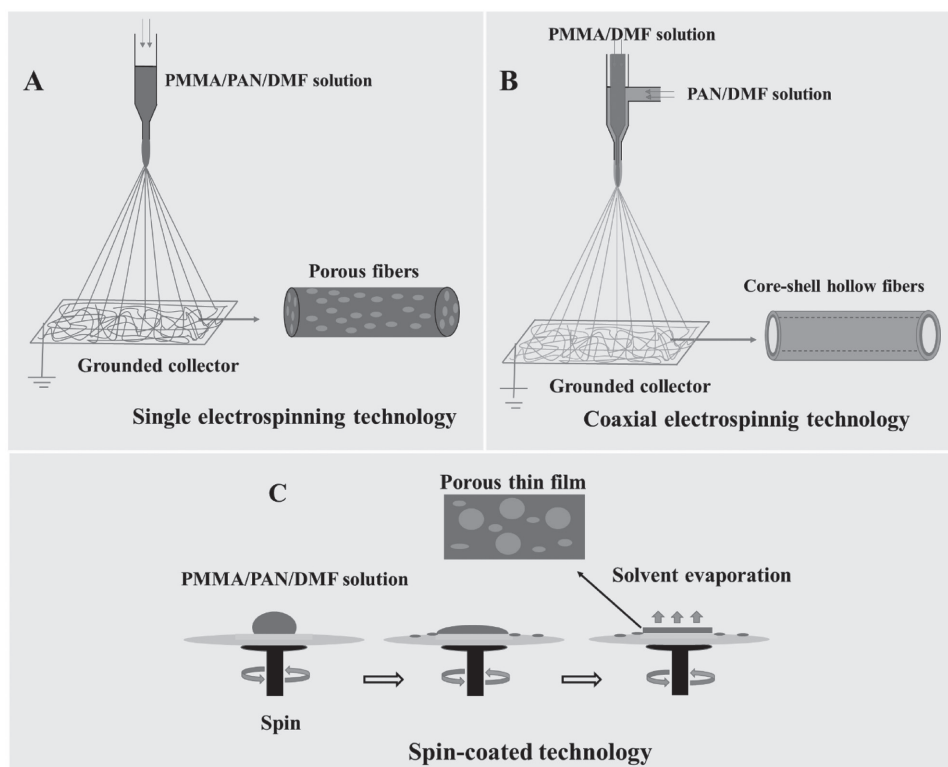
2.2. Preparation of Porous Fibers, Core-Shell Hollow Fibers, and Porous Thin Films

2.2.1. PMMA/PAN Porous Fibers

The PMMA/PAN porous fibers were prepared by single electrospinning technology (Figure 1A). Certain weight of raw PAN (1.6417 g) and PMMA (3.8306 g) powders were dissolved into 20 mL DMF to prepare PAN/PMMA/DMF solution (mass ratio of PAN/PMMA was 3:7). In order to dissolve the chemicals completely, the suspension was stirred fiercely by a magnetic stirrer at room temperature until the solutions were totally transparent. Then, the above solution was injected into 10 mL syringe for electrospinning. The feeding solutions were supplied by the syringe pumps (NE-300, New Era), and the high voltage was supplied by a high voltage source (Gamma High Voltage Research, Product HV power supply, Model No. ES3UP-5w/DAM). The single needle and syringe were used during this process. The syringe was fixed on the syringe pump, and the needle was connected to the high voltage source. The processing parameters were as follows: 15.0 kV (high voltage), 6.0 μL min⁻¹ (feeding flow speed), and 12 cm (distance from needle to the collector). The electrospun fibers were collected by a piece of grounded aluminum foil and then the fibers were dried at 60 °C in the oven over night for solvent evaporation.

2.2.2. PMMA/PAN Core-Shell Hollow Fibers

The PMMA/PAN core-shell hollow fibers were prepared by coaxial electrospinning technology (Figure 1B). A certain amount



■ Figure 1. The schematic diagrams of A) single electrospinning, B) coaxial electrospinning, and C) spin-coating technologies.

of PAN and PMMA were weighted and then added into DMF solvent separately to prepare 8.0 wt% PAN/DMF and 16.0 wt% PMMA/DMF solutions. The suspensions were stirred fiercely by a magnetic stirrer at room temperature until the PAN and PMMA powders were totally dissolved. Two needles and syringes were used during this process. The PMMA (inner) and PAN (outer) solutions were placed into two 10 mL syringes, respectively, which were then fastened onto the syringe pumps. Then, the two needles were linked to a coaxial needle, which was connected with the high voltage source. The processing parameters were shown as follows: 15.0 kV (high voltage), $6.0 \mu\text{L min}^{-1}$ (outer feeding speed), $7.0 \mu\text{L min}^{-1}$ (inner feeding speed), and 12 cm (distance from needle to the collector). The core-shell hollow fibers (mass ratio of PAN/PMMA was 3:7) were collected by a piece of grounded aluminum foil. After electrospinning, the collected fibers were dried at 60°C in the oven over night for solvent evaporation.

2.2.3. PMMA/PAN Porous Thin Films

The transparent PMMA/PAN porous thin films were prepared by spin-coating technology (Figure 1C). The PAN/PMMA/DMF solution (mass ratio of PAN/PMMA is 3:7) was prepared. Then, the above solution was dropped onto a clean glass slide. After the glass slides were placed in the spin coater instrument (CSC 6800 spin coater series), the porous thin films were produced at the speed of 2000 rpm for 30 s. Then, the porous thin films were dried at 60°C in the oven overnight for solvent evaporation.

2.3. Characterizations

2.3.1. Determination of the Functional Groups

Attenuated total reflectance (ATR) infrared spectroscopy was carried out by ATR-IR Spectrometer (Thermo Nicolet 380, Thermoscientific). All the samples were tested in the infrared wavelength range of 400–4000 nm.

2.3.2. Thermal Properties

Thermogravimetric analysis (TGA) was taken by a simultaneous thermal analyzer (6000, PerkinElmer) from 30 to 850°C at a heating rate of $10^\circ\text{C min}^{-1}$ and nitrogen flow rate of 20 mL min^{-1} . The weight loss and derivative weight were recorded during this process. The differential scanning calorimetry (DSC) was performed by a differential scanning calorimeter Q-2000 (TA Instruments). All the samples were heated from 25 to 290°C with the heating and nitrogen flow rates of 2°C min^{-1} and 20 mL min^{-1} , respectively. The values of heat flow at different temperatures were obtained during this period.

2.3.3. Morphological Characterizations

The morphologies of fibers and thin films were characterized by a field emission scanning electron microscope (SEM, LEO 1530VP) operating at 5 kV. The transmission electron microscope (TEM) images were obtained by a FEI Tecnai G2 12 microscope operating at 100 kV and a JEOL JEM2010 microscope operating at 200 kV. The suspended samples in acetone were prepared by ultrasonication, and then were dropped onto a holey carbon coated copper grid to obtain the specimens for TEM.

2.3.4. Crystal Properties

The crystallization of the samples was tested by a desktop X-ray diffractometer (XRD, Rigaku MiniFlexII, Rigaku) with a Cu target X-ray tube and a diffracted beam monochromator limiting the beam to Cu K_{α} radiation. The data was collected in the 2θ range of 5° – 80° .

3. Results and Discussion

3.1. Morphology Study

The diameter of electrospun pure PMMA fibers was about 300–800 nm with smooth surface (Figure 2A). However, the electrospun PAN fibers were observed to have a rough surface with an average diameter of about 400 nm (Figure 2F). The rough surface might be caused by the PAN crystallization, attributing to the DMF evaporation during the electrospinning process.^[47] The porous structure of

PMMA/PAN thin films and fibers (Figure 2B,E) was attributed to the microphase separation structure and the immiscible property between PMMA and PAN.^[34,47] The boundary of PMMA and PAN phases would be formed after DMF evaporation, leading to the porous structure (the schematic diagram was shown in Figure 3).^[48] The diameter of PMMA/PAN porous fibers was about 600–800 nm, and the diameter of pores on the PMMA/PAN porous fibers surface was around 50 nm (Figure 2E). The diameters of large and small pores in the PMMA/PAN thin films were 1–0.8 μm and 200–100 nm, respectively. The PMMA/PAN core-shell hollow fibers were produced by coaxial electrospinning with the outer and inner diameters about 400 and 150 nm, respectively (Figure 2D).

3.2. Functional Group Analysis

ATR-IR spectra of raw PAN and PMMA powders, pure PAN and PMMA electrospun fibers, PMMA/PAN porous fibers

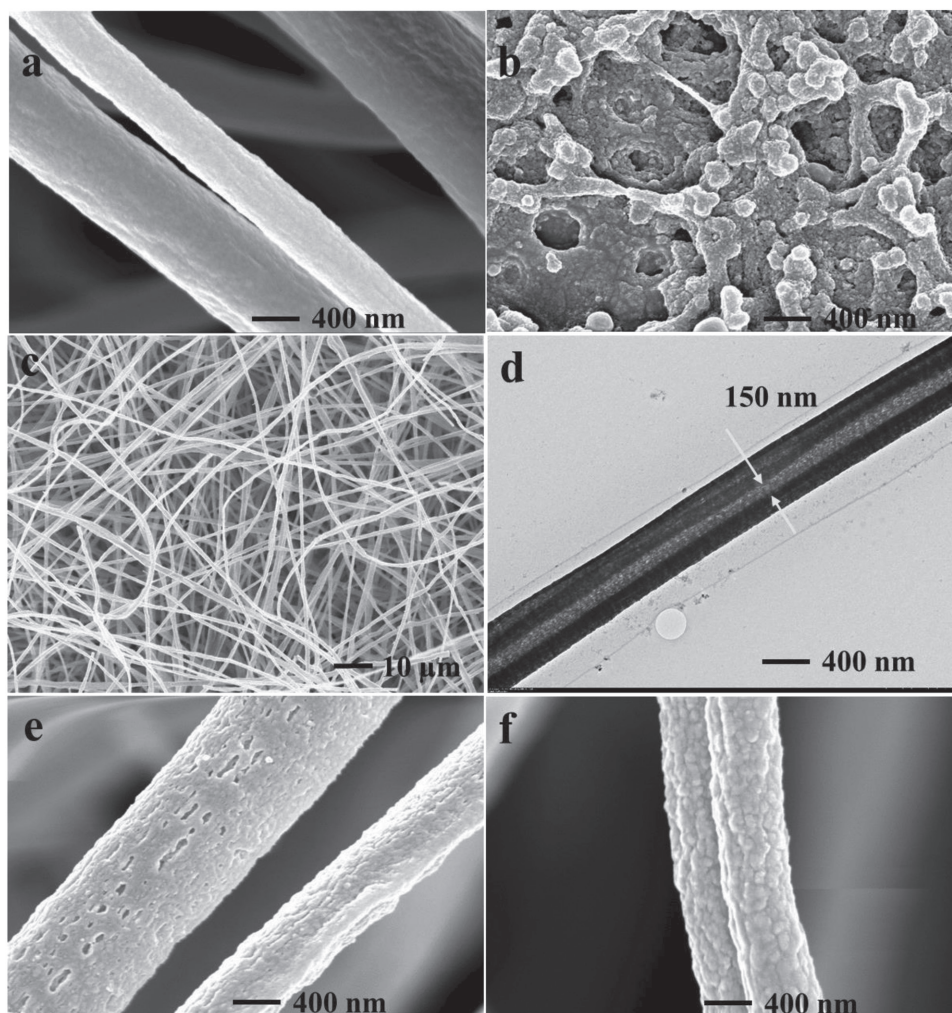


Figure 2. SEM image of A) pure PMMA fibers, B) PMMA/PAN thin film, C) PMMA/PAN core-shell fibers, D) PMMA/PAN core-shell hollow fibers, E) PMMA/PAN blend fibers, and F) pure PAN fibers.

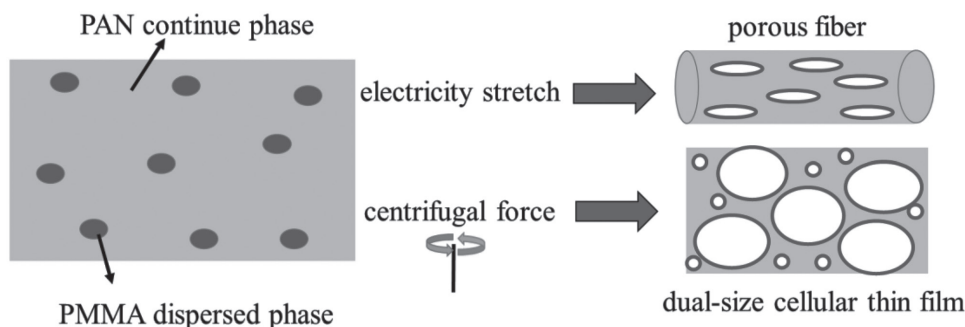


Figure 3. The schematic diagram of the formation of PMMA/PAN porous fibers and thin films.

and thin films, and core-shell hollow PMMA/PAN fibers were obtained to verify the variation of the functional groups (Figure 4). The spectrum of raw PAN powders (Figure 4g), the prominent peaks at 1450 and 2935 cm^{-1} were assigned to the stretch vibration of methylene ($-\text{CH}_2$) group, and the peak at 2246 was due to the stretching nitrile ($-\text{C}\equiv\text{N}$) group.^[49,50] When the PAN was processed into fibers (Figure 4f), the peak at 2340 cm^{-1} ($-\text{C}=\text{N}$ conjugation) displayed stronger intensity, probably due to the cyclization reaction between DMF and PAN.^[49–52] And the stretching nitrile ($\text{C}\equiv\text{N}$) group shifted to higher energy position at 2360 cm^{-1} ($-\text{C}\equiv\text{N}$), ascribing to the interaction of amide nitrogen (DMF) and nitrile group (PAN).^[50–54] The spectra of raw PMMA powder, PMMA fibers, PMMA/PAN porous thin films, core-shell hollow PMMA/PAN fibers, and PMMA/PAN porous fibers showed a weak peak around 999 cm^{-1} and two strong peaks at 1146 and 1726 cm^{-1} , corresponding to the vibrations of C–H, axial asymmetric bend of C=C=O and PMMA ester ($-\text{C}=\text{O}$) groups, respectively

(Figure 4a–e).^[55] The peaks at around 1195–1265 cm^{-1} were obtained due to the C–O–C stretching and deformation vibration.^[55,56] The spectra of the PMMA powders, PMMA fibers, PMMA/PAN porous thin films, core-shell hollow PMMA/PAN fibers, and PMMA/PAN porous fibers showed the obvious peaks at around 2950 and 3002 cm^{-1} , attributing to the C–H bonds stretching vibrations of the $-\text{CH}_2-$ and $-\text{CH}_3$ groups in PMMA (Figure 4c–e).^[57,58] And the peak at 1450 cm^{-1} , at the same position with PAN, was assigned to the C–H vibration of PMMA.^[53] The peak at 2362 cm^{-1} (O–CH₃ stretch) was observed in the PMMA powders, but disappeared in the PMMA fibers (Figure 4b),^[53] which may be caused by the severe synthesis condition (high voltage, 15.0 kV), similar to the synthesis procedure of the silica aerogels.^[59] Furthermore, the peaks (2362 cm^{-1}) of the PAN/PMMA core-shell fibers and porous fibers could be assigned to the stretching nitrile ($-\text{C}\equiv\text{N}$) group of PAN.^[50–54]

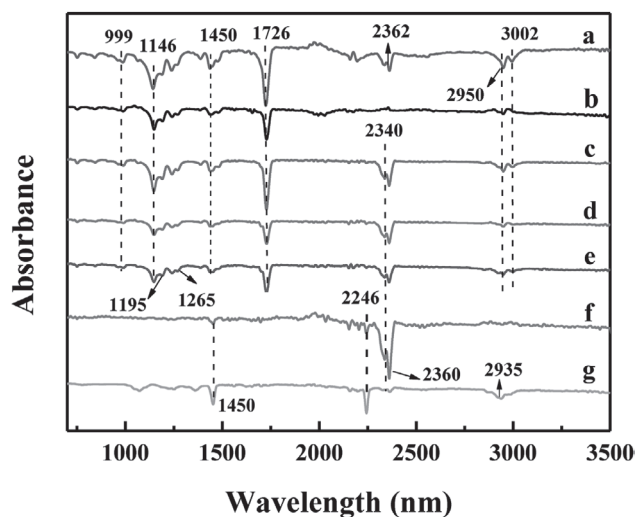


Figure 4. ATR-IR curves of the electrospinning fibers and thin films: (a) pure raw PMMA powder, (b) pure PMMA fibers, (c) PMMA/PAN porous thin films, (d) PMMA/PAN core-shell fibers, (e) PMMA/PAN porous fibers, (f) pure PAN fibers, and (g) pure raw PAN powder.

3.3. Thermal Properties

The thermal stabilization of all the samples was characterized by TGA (Figure 5A), and the weight loss at 850 °C in nitrogen was summarized in Table 1. The raw PMMA powders and pure PMMA fibers were almost degraded at 850 °C under nitrogen atmosphere. For pure raw PAN powders, the final weight loss (54.13%) was lower than that of pure PAN fibers (86.07%) at 850 °C, probably due to the plasticizing effect of residual DMF solvent on the polymer matrix.^[60] Compared with the weight loss at 850 °C of the PMMA/PAN porous fibers (94.45%) and core-shell hollow fibers (91.53%), the weight loss of the PMMA/PAN porous thin films (74.63%) was the lowest, demonstrating that the PMMA/PAN porous thin films were more thermally stable than that of the PMMA/PAN core-shell hollow fibers and porous fibers.

The TGA results with the temperature of the maximum rate of weight loss (inflection point, T_{max}) are shown in Figure 5B. One major thermal degradation was observed obviously in all the samples except pure PAN fibers. As shown in Figure 5C, two major degradation stages in the

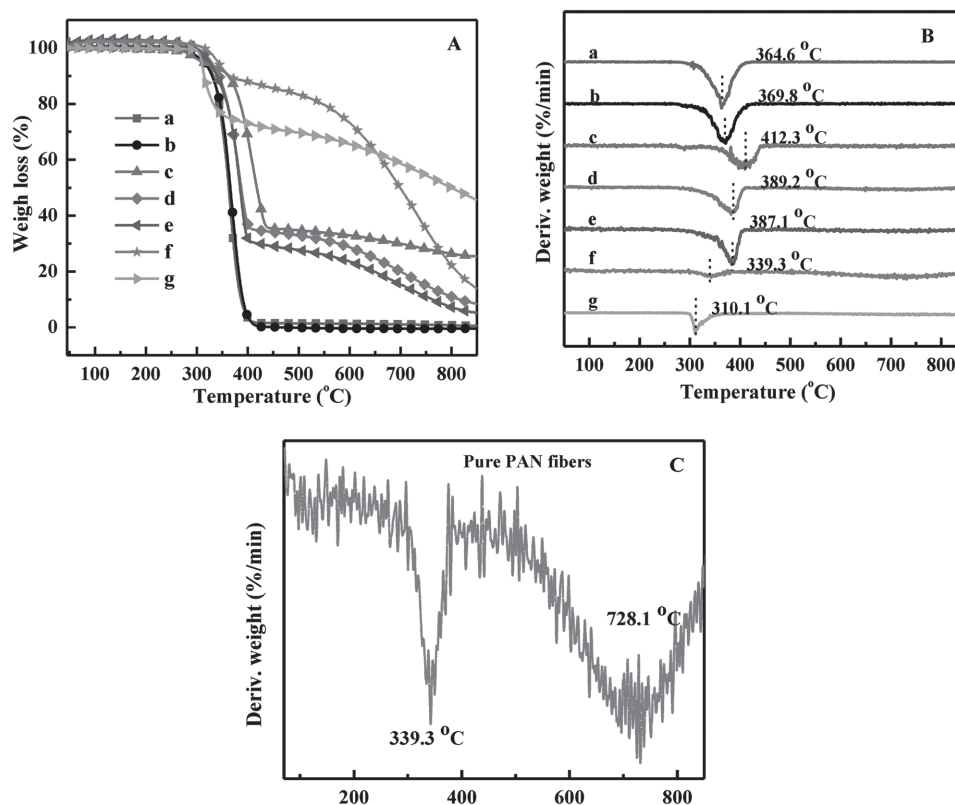


Figure 5. Thermogravimetric analysis (TGA) curves of (a) pure raw PMMA powder, (b) pure PMMA fibers, (c) PMMA/PAN porous thin films, (d) PMMA/PAN core-shell fibers, (e) PMMA/PAN porous fibers, (f) Pure PAN fibers, and (g) pure raw PAN powder. A) Weight percentage, B) derivative weight versus temperature, and C) derivative weight versus temperature of pure PAN fibers.

pure PAN fibers occurred at 280–400 °C and 450–750 °C. The first stage of thermal degradation in PAN was mainly ascribed to the intramolecular nitrile oligomerization and cyclization of nitrile groups, which caused the subsequent chain scission and produced volatile products, such as NH_3 , HCN , CH_3CN .^[61,62] The second degradation stage of PAN occurring at higher temperature was related to the thermal oxidative reactions.^[62] As shown in Figure 5Ba,g, the raw PMMA and PAN powders were degraded at 300–400 °C. In the PMMA, the head-to-head linkages (H–H) was scissile around 165 °C, the C–C

backbone bond was decomposed around 270 °C, and the hemolytic scission β to the vinyl group occurred at around 350 °C.^[63] The inflection point (T_{max}) of pure PAN (339.3 °C, Figure 5Bf) and PMMA fibers (369.8 °C, Figure 5Bf) were higher than that of pure raw PAN (310.1 °C, Figure 5Bg) and PMMA powders (364.6 °C, Figure 5Ba). When PMMA was added into the PAN fibers, the T_{max} of PMMA/PAN porous fibers was higher than that of pure PAN fibers (387.1 °C, Figure 5Be). Furthermore, the T_{max} of porous thin films (412.3 °C, Figure 5Bc) and PMMA/PAN core-shell hollow fibers (389.2 °C, Figure 5Bd) were higher than that of PMMA/PAN porous fibers (Figure 5Be), demonstrating that the morphology of polymers displayed a great effect on their degradation temperature.

The first heating curves of DSC were used to study the thermal properties of products synthesized by different processes (Figure 6A,B). The glass-transition temperatures (T_g) of raw pure PAN powders (94.73 °C, Figure 6Bg) and PMMA powders (115.05 °C, Figure 6Ba) were a little higher than that of pure PAN (93.48 °C, Figure 6Bf) and PMMA fibers (113.84 °C, Figure 6Bb), probably due to the plasticizing effect of residual DMF solvent in the polymer matrix.^[60] However, compared with the T_g of raw PAN powders and pure PAN fibers, the T_g of PMMA/PAN porous fibers (112.69 °C, Figure 6Be), core-shell hollow fibers

Table 1. Weight loss of the investigated materials at 850 °C in nitrogen condition.

Sample	Weight loss [%]
Pure raw PMMA powders	100
Pure PMMA fibers	99.51
PMMA/PAN porous thin films	74.63
PMMA/PAN core-shell hollow fibers	91.53
PMMA/PAN porous fibers	94.45
Pure PAN fibers	86.07
Pure raw PAN powders	54.13

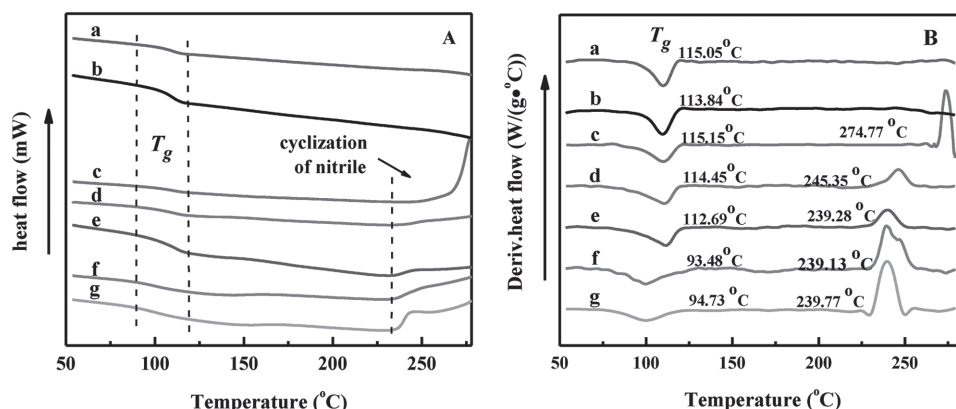


Figure 6. DSC curves of first heating-up period of A) heat flow versus temperature and B) derivative heat flow versus temperature: (a) pure raw PMMA powder, (b) pure PMMA fibers, (c) PMMA/PAN porous thin films, (d) PMMA/PAN core-shell fibers, (e) PMMA/PAN porous fibers, (f) pure PAN fibers, and (g) pure raw PAN powder.

(114.45 °C, Figure 6Bd) and porous thin films (115.15 °C, Figure 6Bc) were increased greatly, which was probably caused by the discontinuous phase of PMMA in the PAN matrix. The discontinuous PMMA with high thermal properties behaved as the nanoparticles in the PAN phases, leading to the improvement of T_g . Particularly, the T_g values of the PMMA/PAN porous thin films and the PMMA/PAN core-shell hollow fibers were higher than that of the PMMA/PAN porous fibers, indicating that different morphologies of products resulted from different processes influenced the transformation of polymer from glassy state to elastomeric state.

The melting temperature (T_m), represented as the endothermic phenomenon of crystal, reflects the crystalline phenomenon of materials.^[31,64] As shown in Figure 6Ba,b, no obvious T_m was observed in raw PMMA powders and pure PMMA fibers, displaying amorphous state of pure PMMA powders and fibers. It was well known that the conventional DSC is difficult to investigate the melting temperature of PAN because of the simultaneous occurrence of cyclization reactions and melting.^[31,65] A sharp exothermic peak was observed above 239 °C (Figure 6Bb–g), attributing to the reactions of PAN cyclization of nitrile groups, dehydrogenation, and oxidation.^[31,63,65] The exothermic temperatures of raw PAN powders, pure PAN fibers, and PMMA/PAN porous fibers relating to the reactions of PAN cyclization of nitrile groups, dehydrogenation, and oxidation were almost the same (Figure 6Be–g), demonstrating that the blending of PMMA into PAN did not affect the PAN reactions of nitrile cyclization, dehydrogenation, and oxidation. However, the temperature of these reactions shifted to higher temperature in PMMA/PAN core-shell hollow fibers (Figure 6Bd) and porous thin films (Figure 6Bc), meaning that the morphologies could affect the temperatures of PAN reactions and caused different thermal stability, subsequently.

3.4. Crystallization Analysis

The XRD patterns of all the samples are shown in Figure 7. The spacing (d) and stacking height (L_c) of lattice planes for charactering the crystalline space (shown in Table 2) were calculated by the Bragg Equation (1) and Scherrer Equation (2), respectively^[66–68]

$$\lambda = 2d \sin \theta \quad (1)$$

$$L_c = \frac{K\lambda}{B \cos \theta} \quad (2)$$

where λ (0.154 nm) represents the wavelength of incident wave. L_c is the mean size of the crystalline domains,

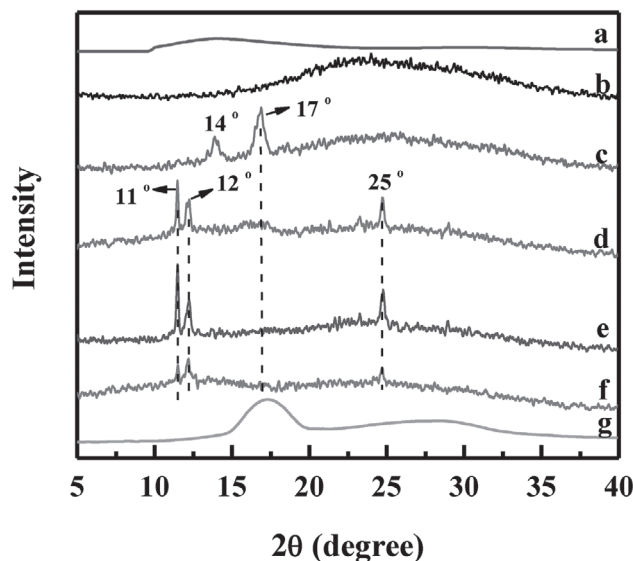


Figure 7. XRD patterns of the electrospinning fibers and porous thin films: (a) pure raw PMMA powder, (b) pure PMMA fibers, (c) PMMA/PAN porous thin films, (d) PMMA/PAN core-shell fibers, (e) PMMA/PAN blend fibers, (f) pure PAN fibers, and (g) pure raw PAN powder.

■ Table 2. The Bragg spacing (d) and stacking height (L_c) of PAN crystals.

Samples	2θ [°]	Spacing, d [Å]	Stacking height, L_c [Å]
PMMA/PAN core-shell hollow fibers	11	7.7017	0.549653715
PMMA/PAN porous fibers	11	7.6894	1.155962563
Pure PAN fibers	11	7.676	0.47499237
PMMA/PAN core-shell hollow fibers	12	7.2258	0.480607127
PMMA/PAN porous fibers	12	7.2141	0.583892273
Pure PAN fibers	12	7.2603	0.359825704
PMMA/PAN porous thin films	14	6.3495	0.364879172
PMMA/PAN porous thin films	17	5.2542	0.307797431
Raw PAN powders	17	5.1498	0.16904746
PMMA/PAN core-shell hollow fibers	25	3.5985	0.616601052
PMMA/PAN porous fibers	25	3.5986	0.665082998
Pure PAN fibers	25	3.6014	0.370240892

which may be smaller or equal to the grain size. K ($K = 1$) is a dimensionless shape factor, B represents full width at half-maximum intensity. As shown in Figure 7a,b, no diffraction peak was observed in the amorphous structure of pure raw PMMA powders and PMMA fibers, which is consistent with the disappearance of melting peak in DSC (Figure 6Ba,b). A diffraction peak at $2\theta = 17^\circ$ was observed in pure raw PAN powders, assigning to the orthorhombic structure of PAN crystals and indexed as (010).^[31,66] The average Bragg spacing (d) of orthorhombic crystals at 17° was found to be 5.1498 Å. For the PMMA/PAN porous thin films, a new peaks at 14° ($d = 6.3495$ Å) appeared (Figure 7c). No diffraction peaks at 17° and 14° were found in pure PAN fibers, porous PMMA/PAN fibers, and PMMA/PAN core-shell hollow fibers. However, three new peaks at 11° , 12° , and 25° were observed, and the average Bragg spacing of above three crystals were about 7.7, 7.2, and 3.6 Å, respectively (Figure 7d–f). The diffraction peak at 25° was attributed to the rotational disorder in intermolecular packing.^[66] These results demonstrated that different processing methods (electrospinning and centrifuge processes) could lead to different types of PAN crystallites.

As shown in Table 2, the Bragg spacing of the same types of crystallites was almost the same in different samples. Compared with pure PAN fibers, the L_c of crystals ($2\theta = 11^\circ$, 12° , and 25°) in the PMMA/PAN porous fibers and PMMA/PAN core-shell hollow fibers were higher than those in pure PAN fibers, and the L_c of crystal ($2\theta = 17^\circ$) in PMMA/PAN porous thin films was higher than that in raw PNA powders, indicating that the adding of PMMA into PAN matrix improved the growth of crystals, and caused the subsequent enhanced stacking height of crystallites. Moreover, the values of crystal L_c at 11° , 12° , and 25° in the PMMA/PAN porous fibers were higher than that in the PMMA/PAN core-shell hollow fibers, demonstrating

that the PAN crystallites in PMMA/PAN porous fibers grew better than those in PMMA/PAN core-shell hollow fibers, which was due to the better corporation of PMMA blend into the PAN matrix in PMMA/PAN porous fibers than that in PMMA/PAN core-shell hollow fibers.

4. Conclusions

The PMMA/PAN porous fibers, core-shell hollow fibers and porous thin films were produced by single electrospinning, coaxial electrospinning, and spin-coating processes, respectively. It is found that the blending of PMMA into PAN matrix can cause porous structures due to the microphase-separation structure of immiscible PMMA and PAN phases. The degradation temperatures of all the samples were 300–400 °C, and the adding of PMMA into PAN led the degradation temperature and T_g shift to higher temperature ranges. Moreover, the lower weight loss, higher degradation temperature and higher T_g of the PMMA/PAN porous thin films than those of the PMMA/PAN porous fibers and core-shell hollow fibers indicated a higher thermal stability of the PMMA/PAN porous thin films. No melting temperature of pure PMMA powders and fibers was observed in DSC due to the amorphous PMMA, and the simultaneous occurrence of PAN reactions (nitrile cyclization, dehydrogenation, and oxidation) and melting led to the sharp exothermic peaks at above 239 °C. However, PMMA did not affect the PAN reactions, since the temperatures of these reactions in pure PAN fibers, PMMA/PAN porous fibers were almost the same at about 239 °C. It was also observed that the higher temperature of reactions in the PMMA/PAN porous thin films than that in the PMMA/PAN core-shell fibers and the PMMA/PAN porous fibers, demonstrated a higher thermal stability of

porous thin films. The same types of PAN crystals ($2\theta = 11^\circ$, 12° , and 25°) in all electrospun fibers, but the PAN crystals ($2\theta = 17^\circ$ and 14°) were observed in the PMMA/PAN porous thin films, indicating that different types of crystals were formed due to different processes. The higher stacking height of PAN crystals at 17° in the PMMA/PAN porous thin films than that in raw PAN powders, and the same situation observed in the PMMA/PAN porous fibers, core-shell hollow fibers, and pure PAN fibers, indicating that the adding of PMMA into PAN can increase the L_c of same types of PAN crystals. Furthermore, the higher stacking height (L_c) of PAN crystals in the PMMA/PAN porous fibers than that in the PMMA/PAN core-shell fibers demonstrated that the better blend of PMMA into PAN matrix enhanced the size of PAN crystals.

Acknowledgements: The authors gratefully acknowledge the financial support from the start-up fund of University of Tennessee. Z. Wang acknowledges NIH under Grant No. 2G12MD007595-06 for support. J. Huang acknowledges the support from China Scholarship Council (CSC) program. Y. Cao acknowledges the support from the National Natural Science Foundation of China (Grant Nos. 21503082), Guangdong Provincial National Science Foundation (Grant No. 2014A030310447), Fundamental Research Funds for the Central Universities of China (Grant No. 2015ZM048), and the China Postdoctoral Science Foundation (Grant No. 2015M572322). X. Peng acknowledges the financial support of the National Natural Science Foundation of China (Grant Nos. 51573063 and 21174044), Guangdong Natural Science Foundation (Grant No. S2013020013855), Guangdong Science and Technology Planning Project (Grant Nos. 2014B010104004 and 2013B090600126), National Basic Research Development Program 973 in China (Grant No. 2012CB025902) and the Research Enhancement Grant of South China University of Technology.

Received: April 11, 2016; Revised: April 23, 2016;
Published online: June 10, 2016; DOI: 10.1002/mame.201600172

Keywords: core-shell hollow fibers; PMMA/PAN; porous fibers; porous thin films

- [1] C. W. Frank, V. Rao, M. M. Despotopoulou, R. F. W. Pease, W. D. Hinsberg, R. D. Miller, J. F. Rabolt, *Science* **1996**, 273, 912.
- [2] M. S. Lavine, *Science* **2015**, 348, 408.
- [3] D.-W. Wang, F. Li, J. Zhao, W. Ren, Z.-G. Chen, J. Tan, Z.-S. Wu, I. Gentle, G. Q. Lu, H.-M. Cheng, *ACS Nano* **2009**, 3, 1745.
- [4] M. Peng, D. Li, L. Shen, Y. Chen, Q. Zheng, H. Wang, *Langmuir* **2006**, 22, 9368.
- [5] E. Zussman, A. L. Yarin, A. V. Bazilevsky, R. Avrahami, M. Feldman, *Adv. Mater.* **2006**, 18, 348.
- [6] J. Zhu, S. Wei, J. Ryu, M. Budhathoki, G. Liang, Z. Guo, *J. Mater. Chem.* **2010**, 20, 4937.
- [7] J. Zhu, S. Wei, X. Chen, A. B. Karki, D. Rutman, D. P. Young, Z. Guo, *J. Phys. Chem. C* **2010**, 114, 8844.
- [8] X. Chen, S. Wei, C. Gunesoglu, J. Zhu, C. S. Southworth, L. Sun, A. B. Karki, D. P. Young, Z. Guo, *Macromol. Chem. Phys.* **2010**, 211, 1775.
- [9] H. Jiang, Y. Hu, P. Zhao, Y. Li, K. Zhu, *J. Biomed. Mater. Res. Part B* **2006**, 79, 50.
- [10] H. Jiang, Y. Hu, Y. Li, P. Zhao, K. Zhu, W. Chen, *J. Controlled Release* **2005**, 108, 237.
- [11] L. Hu, M. Pasta, F. L. Mantia, L. Cui, S. Jeong, H. D. Deshazer, J. W. Choi, S. M. Han, Y. Cui, *Nano Lett.* **2010**, 10, 708.
- [12] Y. Picó, M. Fernández, M. J. Ruiz, G. Font, *J. Biochem. Biophys. Methods* **2007**, 70, 117.
- [13] L. Yue, J. Zhang, Z. Liu, Q. Kong, X. Zhou, Q. Xu, J. Yao, G. Cui, *J. Electrochem. Soc.* **2014**, 161, A1032.
- [14] H. Pan, Y. Zhang, Y. Hang, H. Shao, X. Hu, Y. Xu, C. Feng, *Biomacromolecules* **2012**, 13, 2859.
- [15] H. Qu, S. Wei, Z. Guo, *J. Mater. Chem. A* **2013**, 1, 11513.
- [16] Z. Liuxue, L. Peng, S. Zhixing, *Mater. Chem. Phys.* **2006**, 98, 111.
- [17] C. Wang, K.-W. Yan, Y.-D. Lin, P. C. H. Hsieh, *Macromolecules* **2010**, 43, 6389.
- [18] M. Graeser, E. Pippel, A. Greiner, J. H. Wendorff, *Macromolecules* **2007**, 40, 6032.
- [19] X. Zhou, L. Yue, J. Zhang, Q. Kong, Z. Liu, J. Yao, G. Cui, *J. Electrochem. Soc.* **2013**, 160, A1341.
- [20] K. Kanehori, K. Matsumoto, K. Miyauchi, T. Kudo, *Solid State Ionics* **1983**, 9, 1445.
- [21] S.-W. Kim, G.-H. Kim, *Appl. Opt.* **1999**, 38, 5968.
- [22] H. C. Tsai, D. Bogy, *J. Vac. Sci. Technol. A* **1987**, 5, 3287.
- [23] M. Weisheit, S. Fähler, A. Marty, Y. Souche, C. Poinignon, D. Givord, *Science* **2007**, 315, 349.
- [24] M. E. Davis, *Nature* **2002**, 417, 813.
- [25] A. Walcarius, A. Kuhn, *TrAC-Trends Anal. Chem.* **2008**, 27, 593.
- [26] K. Akimoto, S. Ishizuka, M. Yanagita, Y. Nawa, G. K. Paul, T. Sakurai, *Sol. Energy* **2006**, 80, 715.
- [27] W. Jeong, S. Kim, G. Park, *Thin Solid Films* **2006**, 506, 180.
- [28] J. Zhang, Z. Liu, Q. Kong, C. Zhang, S. Pang, L. Yue, X. Wang, J. Yao, G. Cui, *ACS Appl. Mater. Interfaces* **2013**, 5, 128.
- [29] S. Dalton, F. Heatley, P. M. Budd, *Polymer* **1999**, 40, 5531.
- [30] D. Grosjean, E. Grosjean, E. L. Williams, *Air Waste* **1994**, 44, 391.
- [31] Y. Furushima, M. Nakada, H. Takahashi, K. Ishikiriyama, *Polymer* **2014**, 55, 3075.
- [32] P. Wang, *J. Appl. Polym. Sci.* **1998**, 67, 1185.
- [33] T. J. Xue, M. A. McKinney, C. A. Wilkie, *Polym. Degrad. Stab.* **1997**, 58, 193.
- [34] N. C. Abeykoon, J. S. Bonso, J. P. Ferraris, *RSC Adv.* **2015**, 5, 19865.
- [35] Y. Wu, M. Gao, X. Li, Y. Liu, H. Pan, *J. Alloys Compd.* **2014**, 608, 220.
- [36] C. Bohn, J. Schaefgen, W. Statton, *J. Polym. Sci.* **1961**, 55, 531.
- [37] A. V. Bazilevsky, A. L. Yarin, C. M. Megaridis, *Langmuir* **2007**, 23, 2311.
- [38] Z. Sun, E. Zussman, A. L. Yarin, J. H. Wendorff, A. Greiner, *Adv. Mater.* **2003**, 15, 1929.
- [39] M. Yanilmaz, X. Zhang, *Polymers* **2015**, 7, 629.
- [40] W. S. Khan, R. Asmatulu, V. Rodriguez, M. Ceylan, *Int. J. Energy Res.* **2014**, 38, 2044.
- [41] D. Li, J. T. McCann, Y. Xia, *Small* **2005**, 1, 83.
- [42] J. T. McCann, M. Marquez, Y. Xia, *J. Am. Chem. Soc.* **2006**, 128, 1436.
- [43] Z. Qi, H. Yu, Y. Chen, M. Zhu, *Mater. Lett.* **2009**, 63, 415.
- [44] Y. Zhang, J. Li, G. An, X. He, *Sens. Actuators B* **2010**, 144, 43.
- [45] X. Chen, M. Qiao, S. Xie, K. Fan, W. Zhou, H. He, *J. Am. Chem. Soc.* **2007**, 129, 13305.
- [46] G. Ma, D. Yang, J. Nie, *Polym. Adv. Technol.* **2009**, 20, 147.

- [47] C. K. Hong, K. S. Yang, S. H. Oh, J. H. Ahn, B. H. Cho, C. Nah, *Polym. Int.* **2008**, *57*, 1357.
- [48] E. Jo, J. G. Yeo, D. K. Kim, J. S. Oh, C. K. Hong, *Polym. Int.* **2014**, *63*, 1471.
- [49] F. Nacimiento, R. Alcántara, J. R. González, J. L. Tirado, *J. Electrochem. Soc.* **2012**, *159*, A1028.
- [50] T. H. Ko, H. Y. Ting, C. H. Lin, *J. Appl. Polym. Sci.* **1988**, *35*, 631.
- [51] S. Cetiner, H. Karakas, R. Ciobanu, M. Olariu, N. U. Kaya, C. Unsal, F. Kalaoglu, A. S. Sarac, *Synth. Met.* **2010**, *160*, 1189.
- [52] M. A. Phadke, D. A. Musale, S. S. Kulkarni, S. K. Karode, *J. Polym. Sci. Part B: Polym. Phys.* **2005**, *43*, 2061.
- [53] E. Ghorbel, I. Hadriche, G. Casalino, N. Masmoudi, *Materials* **2014**, *7*, 375.
- [54] A. A. Khan, U. Baig, *Polym. Eng. Sci.* **2013**, *53*, 2027.
- [55] N. S. Pereira, M. J. Sales, A. M. Ceschin, *Polímeros* **2012**, *22*, 384.
- [56] J. Z. Mbese, P. A. Ajibade, *Polymers* **2014**, *6*, 2332.
- [57] A. H. Yuwono, B. Liu, J. Xue, J. Wang, H. I. Elim, W. Ji, Y. Li, T. J. White, *J. Mater. Chem.* **2004**, *14*, 2978.
- [58] O. P. Garcia, M. C. C. d. Albuquerque, K. A. d. S. Aquino, P. L. B. d. Araujo, E. S. d. Araujo, *Mater. Res.* **2015**, *18*, 365.
- [59] W. Li, R. J. Willey, *J. Non-Cryst. Solids* **1997**, *212*, 243.
- [60] N. Passerini, D. Q. M. Craig, *J. Controlled Release* **2001**, *73*, 111.
- [61] M. Surianarayanan, R. Vijayaraghavan, K. Raghavan, *J. Polym. Sci. Part A: Polym. Chem.* **1998**, *36*, 2503.
- [62] D. Gupta, J. Agrawal, R. Sharma, *J. Appl. Polym. Sci.* **1989**, *38*, 265.
- [63] M. Ferriol, A. Gentilhomme, M. Cochez, N. Oget, J. L. Mieloszynski, *Polym. Degrad. Stab.* **2003**, *79*, 271.
- [64] H. S. Kim, *J. Polym. Sci. Part B: Polym. Phys.* **1996**, *34*, 1181.
- [65] S. Xiao, W. Cao, B. Wang, L. Xu, B. Chen, *J. Appl. Polym. Sci.* **2013**, *127*, 3198.
- [66] X. D. Liu, W. Ruland, *Macromolecules* **1993**, *26*, 3030.
- [67] P. J. Sánchez-Soto, M. A. Avilés, J. C. del Río, J. M. Ginés, J. Pascual, J. L. Pérez-Rodríguez, *J. Anal. Appl. Pyrolysis* **2001**, *58-59*, 155.
- [68] S. M. Badawy, A. M. Dessouki, *J. Phys. Chem. B* **2003**, *107*, 11273.